We are IntechOpen, the world's leading publisher of Open Access books
Built by scientists, for scientists

6,900
Open access books available

185,000
International authors and editors

200M
Downloads

154
Countries delivered to

Our authors are among the

TOP 1%
most cited scientists

12.2%
Contributors from top 500 universities

CLARIVATE ANALYTICS
BOOK CITATION INDEX
INDEXED

WEB OF SCIENCE™

Selection of our books indexed in the Book Citation Index
in Web of Science™ Core Collection (BKCI)

Interested in publishing with us?
Contact book.department@intechopen.com

Numbers displayed above are based on latest data collected.
For more information visit www.intechopen.com

Porous Silicon Integrated Photonic Devices for Biochemical Optical Sensing

Ilaria Rea[1], Emanuele Orabona[1,2], Ivo Rendina[1] and Luca De Stefano[1]
[1]Institute for Microelectronics and Microsystems -
Unit of Naples Research National Council, Naples
[2]Dept. of Physics, University of Naples "Federico II", Naples
Italy

1. Introduction

In the last few years, great efforts have been spent in the development of integrated microsystems, devices of few square centimeters in size including microsensors, microfluidic components, reaction chambers, detectors, and so on. More than a simple ensemble of devices, this is a new research field that combines the properties and characteristics of different materials to find innovative and affordable solutions in applications such as sensing, biotechnology, analytical chemistry. The device miniaturization not only means lower costs through mass production, but also improvement in terms of analysis time, simplicity of use and decrease in consumption of materials (reagents and analytes) (Chandrasekaran et al., 2007). The integrated devices are largely made of silicon but can also include a microfluidic systems; for this reason, their technology is based both on the techniques used in integrated circuit manufacturing and on "soft" fabrication methods (Xia & Whitesides, 1998).

In this chapter, we describe the fabrication and the characterization of integrated photonic devices based on nanostructured silicon for biochemical optical sensing. The porous silicon (PSi) is fabricated by electrochemical etching of doped crystalline silicon in an aqueous solution of hydrofluoridric acid. It can be simply described as a network of air holes in a silicon matrix: its dielectric properties, and in particular the refractive index, depend on the content of void, which can be accurately controlled by tuning the process parameters, so that different structures (Fabry-Perot interferometer, Bragg mirror, optical microcavity, aperiodic multilayered sequences) showing good quality optical responses can be obtained. Like other porous materials, PSi is an ideal platform for biosensing due to its high specific surface area ($\sim$100 $m^2 \cdot cm^{-3}$) which assures an efficient interaction with the species to detect. However, the integration of PSi sensing structures in a microsystem is not straightforward: its surface instability and the low compatibility with alkaline treatments, frequent in devices fabrication, are severe limitations in this application field. In this chapter, we analyze these technological limits and propose solutions that have led to the realization of innovative and high-performant integrated devices using porous silicon as functional platform in bio-analysis experiments.

2. Properties of porous silicon

PSi is a very versatile material due to its peculiar morphological, physical, and chemical properties: evidence of this is the huge number of papers about PSi features and devices

based on this nanostructured material that appear in the literature every year. One reason for this clear success is the easy fabrication of sophisticated optical multilayers, such as one-dimensional photonic crystals, by a simple, but not trivial, computer-controlled electrochemical etching process.

2.1 Porous silicon fabrication by electrochemical etching

Porous silicon was discovered in 1956 by the Uhlirs at Bell Labs, USA, during a study on the electropolishing of crystalline silicon in an HF-based solution. They observed the formation of a deposit "tentatively supposed to be a Si suboxide" (Uhlir, 1956). The scientific community was not much interested in porous silicon until to 1990 when Leigh Canham, working at the Defence Research Energy in England, demonstrated an efficient tunable room temperature light output from the material (Canham, 1990). In the years later, thousands of papers were published on porous silicon and its potential applications in microelectronics, optoelectronic devices, chemical and biological sensing.
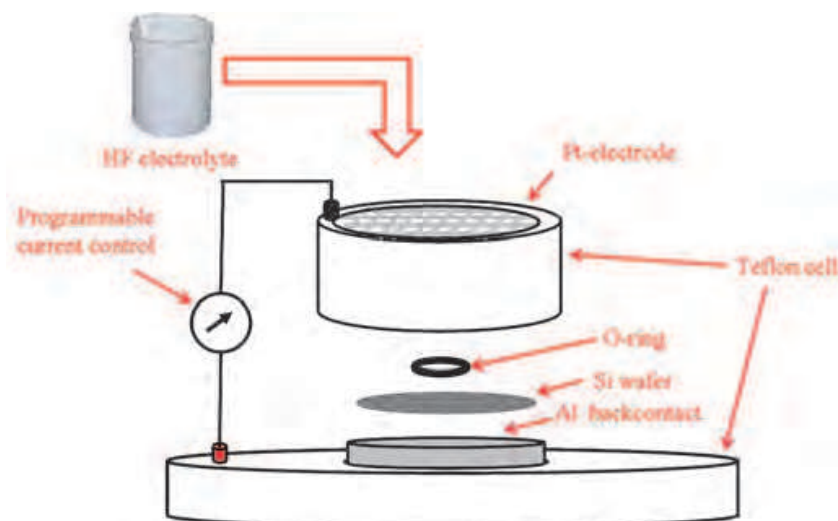

Fig. 1. Electrochemical etching setup.

In most cases, the porous silicon structure is formed by electrochemical dissolution of doped crystalline silicon wafers in hydrofluoric acid (HF) based solution. The cell used for the electrochemical etching is schematized in Figure 1. The silicon wafer is the anode; it is placed in back-side contact on an aluminum plate while the front side is sealed with an O-ring and exposed to the anodising electrolyte. The cathode is made of platinum. The anodisation cell is made of a highly-acid resistant polymer such as polyvinylidene fluoride (PVDF) or polytetrafluoroethylene (PTFE). For highly resistive silicon substrate (> few mΩ/cm) an evaporated metal backside contact is necessary to ensure the Schottky contact between the aluminum plate and the semiconductor.

Figure 2 shows the anodic I-V curve of silicon in HF based solution; the different dissolution regions of the curve are labeled A-C. Pore formation takes place in region A. At anodic overpotentials in excess of the current "peak," region C, silicon electropolishes. At intermediate overpotentials, region B, a "transition" zone exists where pore formation and electropolishing compete for control over the surface morphology. The resulting structure within this region is generally porous in nature but the pore diameters increase rapidly as the electropolishing potential is approached.
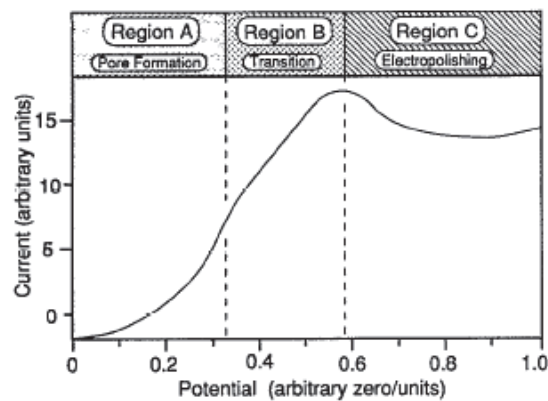
Fig. 2. Anodic I-V curve for silicon in HF. In the region A pore formation occurs. In region C there is the silicon electropolishing. The region B is a transition zone where pore formation and electropolishing compete (Smith & Collins, 1992).
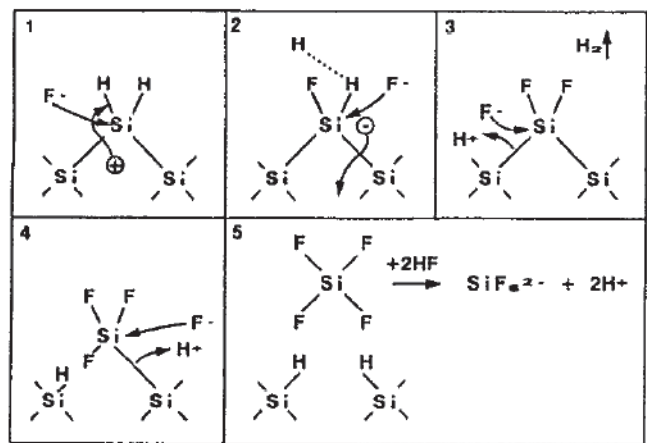

Fig. 3. Dissolution mechanism of silicon in hydrofluoridric acid (HF) (Lehmann & Gösele, 1991).

The exact dissolution chemistries of silicon are still in question, although it is generally accepted that holes are required in the initial steps for both electropolishing and pore formation. The Figure 3 illustrates the chemical dissolution mechanism suggested by Lehmann and Gösele ((Lehmann & Gösele, 1991), that has received great attention. If a hole of the silicon substrate has the sufficient energy to reach the surface, a nucleophilic attack on Si-H bond by fluoride ion can occur and a Si-F bond is formed (step 1 in Figure 3). Due to the polarizing influence of the Si-F bond, another F– ion can attack and bond under generation of an H_2 molecule and injection of one electron into the substrate (steps 2 and 3). The polarization induced by the Si-F groups reduces the electron density of the Si-Si backbonds; these weakened bonds will now be attacked by HF or H_2O (step 4) in a way that the silicon surface atoms remain bonded to hydrogen atoms (step 5). The silicon tetrafluoride molecule reacts with the HF to form the highly stable H_2SiF_6.

In the case of n-type silicon, where holes are minority carriers, the electrochemical dissolution of the material strongly depends on the hole/electron pair generation by

illumination. In fact, when lightly doped (majority carrier concentration below $\sim 10^{18}$ cm^{-3}) n-type silicon is anodised in the dark, the formation of PSi is observed only at high voltages (>5 V). If the anodisation is perform under illumination, PSi is formed at lower potentials (<1 V).

2.2 Porous silicon morphology

The PSi shows a great variety of morphologies dependent on the doping type and level of the silicon substrate and the electrochemical etching parameters. Usually for a given substrate and electrolyte, only one type of pore structure can be obtained.

The IUPAC (International Union of Pure and Applied Chemistry) guidelines define ranges of pore sizes that exhibit characteristic absorption properties (Sing et al., 1985): pores characterized by a diameter ≤ 2nm define microporous silicon; for sizes in the range 2-50 nm the PSi is mesoporous; pores diameters > 50 nm are typical of macroporous silicon.

Highly doped (10^{19} cm^{-3}) p- or n- silicon anodized in aqueous HF solution usually forms mesopores with pore sizes from 20 nm to 50 nm (Figure 4 (a)). Several groups have demonstrated that complex optical devices can be designed with mesoporous silicon (Mulloni & Pavesi, 2000). In the case of lightly doped (below $\sim 10^{18}$ cm^{-3}) p-type silicon, the porous size distribution is normally found in the range 1 – 5 nm, in the lower limit for mesopores (Figure 4 (b)). The influence of the HF concentration has been studied (Ruike et al., 1996): it has been found that the pore size distribution broadens and the mean pore radius increases when the HF concentration in the etching solution is decreased from 55 to 37 %, but no significant changes are observed for lower HF concentrations. The electrochemical etching of lightly doped n-type substrates in the dark results in the formation of a macroporous material with radii in the micrometer range. Under sample illumination mesopores and/or micropores are formed, whereas macropores are still found (Figure 4 (c)).

2.3 Porosity and refractive index determination

The most important parameter of the PSi is the porosity, defined as the fraction of void within the porous layer. The easiest way to determine the porosity is by weight measurements. The wafer is weighed before the anodic reaction (m_1), after the anodic reaction (m_2) and finally after dissolution of the porous material in a molar NaOH aqueous solution (m_3). The porosity is given by the equation:

$$P = \frac{m_1 - m_2}{m_1 - m_3} \tag{1}$$

After the removal of the porous layer, it is also possible to determine its thickness by profilometric analysis. Another interesting technique, that allows to determine simultaneously both the thickness and the porosity of a PSi layer without destroying the material is the spectroscopic ellipsometry (SE) (Tompkins & McGaham, 1999). The method is based on the measurement of the change in the polarization state of the light over the spectral range after the reflection from the sample surface. Ellipsometry measures the complex reflectance ratio (ρ) defined by:

$$\rho = \frac{R_p}{R_s} = \tan\psi e^{i\Delta} \tag{2}$$
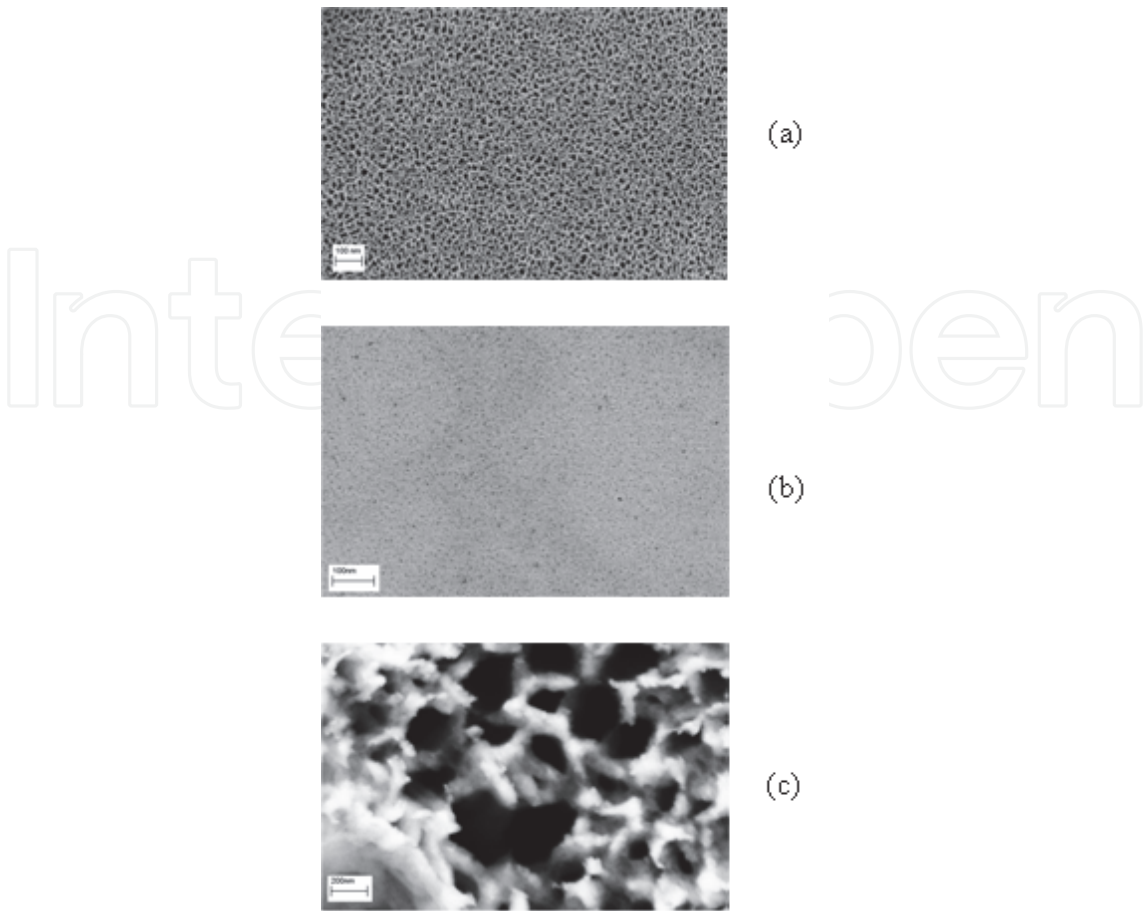
Fig. 4. SEM images illustrating different PSi morphologies. (a) p+ <100> silicon; the pores have an average width of 30 nm. (b) p <100> silicon; the pores size is about 2 nm. (c) n <100> silicon; the material consists of two parts, micro and macropores are found.

where R_p and R_s are the complex reflection coefficients of the light polarized parallel and perpendicular to the plane of incidence. Thus, ψ and Δ are, respectively, the amplitude ratio and the phase shift between s and p components of polarized light. From experimentally determined ρ, it is possible to obtain information about the properties of the material by performing proper model calculations. The use of SE in the near IR-UV spectral range for studying PSi has been largely reported in literature (Zangooie et al., 1999; Pickering et al., 1993). The PSi can be modeled by using a sequence of sublayers, each one constituted by air and crystalline silicon, in order to take into account the inhomogeneity along the layer normal (Zangooie et al., 1998) and adopting the Bruggeman effective medium approximation (EMA) (Aspnes et al., 1979) given in the Eq. 3:

$$(1-P)\left(\frac{\varepsilon_{Si} - \varepsilon_{PSi}}{\varepsilon_{Si} + 2\varepsilon_{PSi}}\right) + P\left(\frac{\varepsilon_{void} - \varepsilon_{PSi}}{\varepsilon_{void} + 2\varepsilon_{PSi}}\right) = 0 \tag{3}$$

where P, ε_{si}, ε_{PSi}, and ε_{void} are the layer porosity, the dielectric constants of silicon, porous silicon and void, respectively. This approximation is acceptable because the size of the PSi pores is much smaller than the wavelengths of incidence light in the near IR-UV regions; in this range, the electromagnetic radiation does not distinguish between silicon and void, and it is possible to treat the PSi as a homogeneous medium.
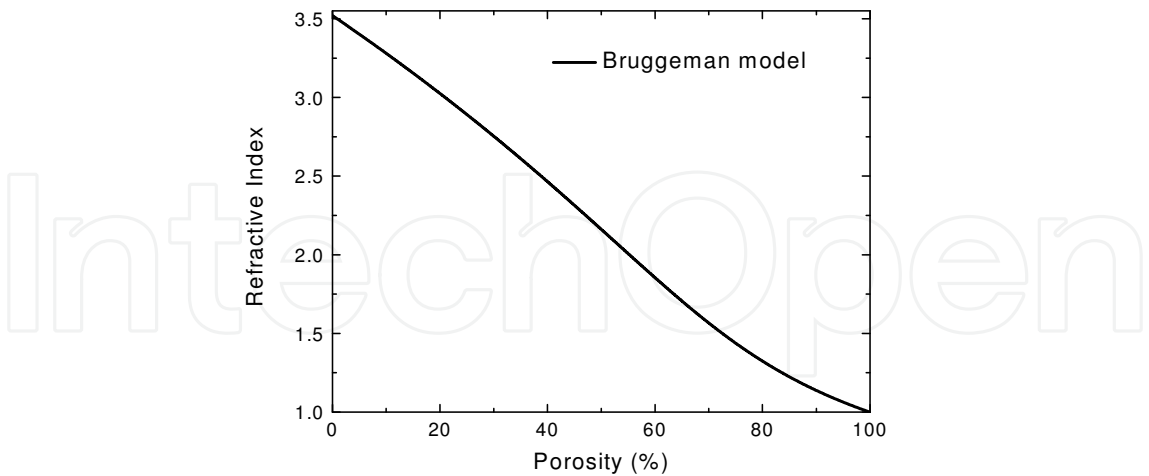
Fig. 5. Dependence of the PSi refractive index on the porosity given by the Bruggeman effective medium approximation.

The root square of the dielectric constant is the complex refractive index, $\tilde{n}=n+ik$ where n is the refractive index and the imaginary part k is the extinction coefficient. k is related to a, the linear absorption coefficient, by the relation $k=a\lambda/4\pi$ where λ is the optical wavelength. The Figure 5 shows the dependence of the PSi refractive index on porosity given by the Bruggeman model.

2.4 Thermal oxidation of porous silicon

The PSi is a material characterized by a high chemical reactivity; if stored in ambient air, the texture becomes partially oxidized and both the refractive index and the extinction coefficient change. To stabilize the PSi and eliminate the problem of aging, the thermal oxidation of the structure is used. The oxidation reduces or completely removes the Si from the skeleton substituting it by SiO_2, that isotropically grows also into the pores. The Figure 6 shows the SEM images of PSi layer (a) and oxidized PSi layer (b).
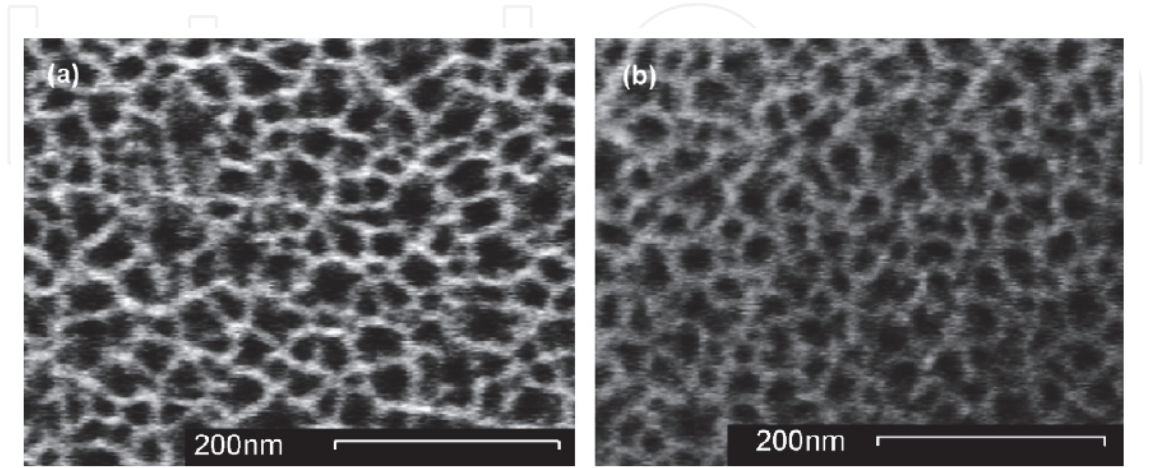

Fig. 6. SEM images of p$^+$ PSi layer (a) and p+ PSi layer pre-oxidized at 300°C for one hour following by an oxidation step at 900 °C in wet O_2 for 1 hour (b) (Pirasteh et al., 2006).

It is possible to observe that after the oxidation the pore shape is conserved but the size is reduced. In particular, the mean value of the pores width from 18 nm becomes 13 nm. Since the pores density is the same and the pore size decreased, the porosity after oxidation is lower than the porosity before oxidation (Pirasteh et al., 2006). The relationship between the porosities of a PSi layer before and after the thermal oxidation is expressed by the equation:

$$(1 - P_{ox}) = (1 + 1.27x)(1 - P) \tag{4}$$

where P is the porosity before oxidation, P_{ox} the porosity after the oxidation and x is the oxidation extent which is a function of the temperature T and the duration t of the process:

$$x(T, t) = 0.44 \left(\frac{SiO_{2\,final}}{Si_{initial}} \right) \tag{5}$$

PSi is generally oxidized in a pure O_2 atmosphere by a two step thermal treatment. The first oxidation step, defined as pre-oxidation, at low temperature (300 - 400 °C) is required in order to selectively oxidise the silicon backbonds thus assuring an easy propagation of the oxidant into the silicon structure (Yon et al., 1987). Moreover, the pre-oxidation reduces the damage of the material texture in the second oxidation step at higher temperatures between 800 and 900 °C (Pap et al., 2005).
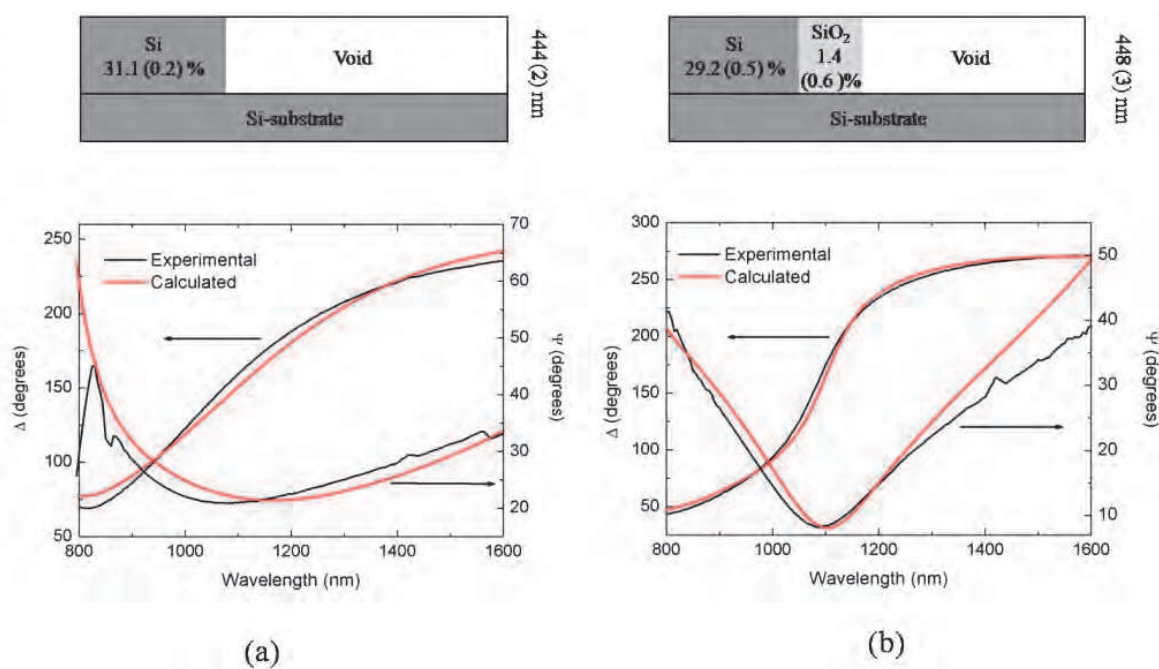

Fig. 7. Schematic diagram of the model layer used in the ellipsometric analysis and calculated ψ, Δ spectra compared with the experimental ones before (a) and after (b) the pre-oxidation at 400° C for 30 min of the p+ PSi layer.

A p+ PSi layer pre-oxidised at 400°C for 30 min has been characterized by spectroscopic ellipsometry before and after the thermal process. In Figure 7 are reported the schematic diagrams of the models used in the analysis and the calculated ψ and Δ spectra compared with the experimental ones before (a) and after (b) the pre-oxidation of the material. The value of the variable x has been estimated to be about 0.02; the oxidation interests only the

surface of the material. A short (3-5 min) thermal treatment at 900°C completely oxidized the structure; in this case x=1 and the Eq. 5 becomes *(1-P_{ox}) = 2.27(1-P)*.

3. Porous silicon photonic devices

In the last few years, PSi resonant photonic structures as Fabry-Perot interferometers (Dancil et al., 1999), Bragg reflectors (Snow et al., 1999), optical microcavities (De Stefano et al., 2003), and Thue-Morse sequences (Moretti et al., 2006) have been intensively studied by several research groups in particular for their photonic properties as interference filters.
The refractive index profile of a PSi multilayered structure can be realized by choosing the proper current density profile during the electrochemical etching of crystalline silicon. This is possible because the PSi fabrication process is self-stopping; an as etched PSi layer is depleted of holes and any further etching only occurs at the pores tips (Lehman, 2002). In this section the PSi optical structures, fabricated for experimental purposes, are described.

3.1 Fabry perot interferometer

A single layer of PSi optically acts as a Fabry-Perot interferometer. In Figure 8 (a) the reflectivity spectrum of a PSi layer under white light illumination is reported. The maxima in the reflectivity spectrum appear at wavelengths λ_m which satisfy:

$$m = 2nd / \lambda_m \qquad (6)$$

where m is an integer, d is the film thickness and n is the average refractive index of the layer (Lin et al., 1997; Anderson et al., 2003). Assuming that the refractive index is independent on the wavelength over the considered range, the maxima are equally spaced in the wavenumber ($1/\lambda_m$). When m maxima are plotted as a function of the wavenumber, each point lies on a straight line whose slope is two times the optical path of the interferometer, as it is shown in the Figure 8 (b).
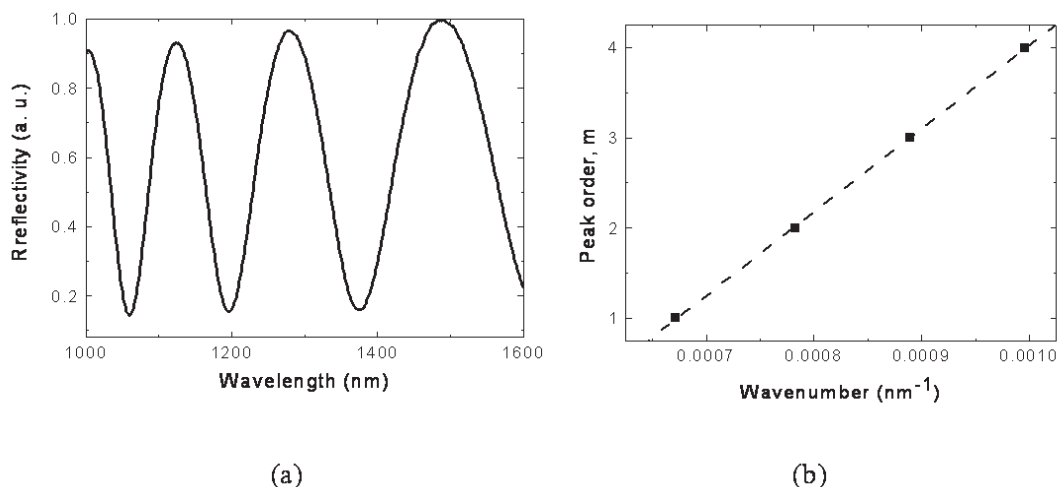

(a)   (b)

Fig. 8. (a) Reflectivity spectrum of a PSi layer realized by the electrochemical etching of p+ crystalline silicon in a solution of 15 % hydrofluoric acid applying a current density of 115 mA/cm² for 11 s (P=69 %; n=1.593 @1.2 µm; d=2.9 µm); (b) m-order peaks are plotted as function of the wavenumber. The optical path of the interferometer has been estimated to be (4620±40) nm.

3.2 Bragg mirror and optical microcavity

The Bragg mirror is a periodic structure made alternating layers of high (n_H) and low (n_L) refractive index, whose thicknesses satisfy the relation $2(n_H d_H + n_L d_L)=m\lambda_B$, where m is the order of the Bragg condition (Figure 9 (a)). The layer stack is usually denoted as [HL]N, where N is the number of periods. The periodicity gives to the structure a photonic band gap (PBG) behavior characterized by the property to forbid the transmission of the light at fixed wavelengths. The reflectivity spectrum of a Bragg mirror is thus characterized by the presence of a stop band centered around the Bragg wavelength λ_B (Figure 9 (b)). For a given number of periods, the height and width of the reflectivity stop band increases by increasing the index ratio H/L. A low index contrast can be compensated by a higher number of periods.
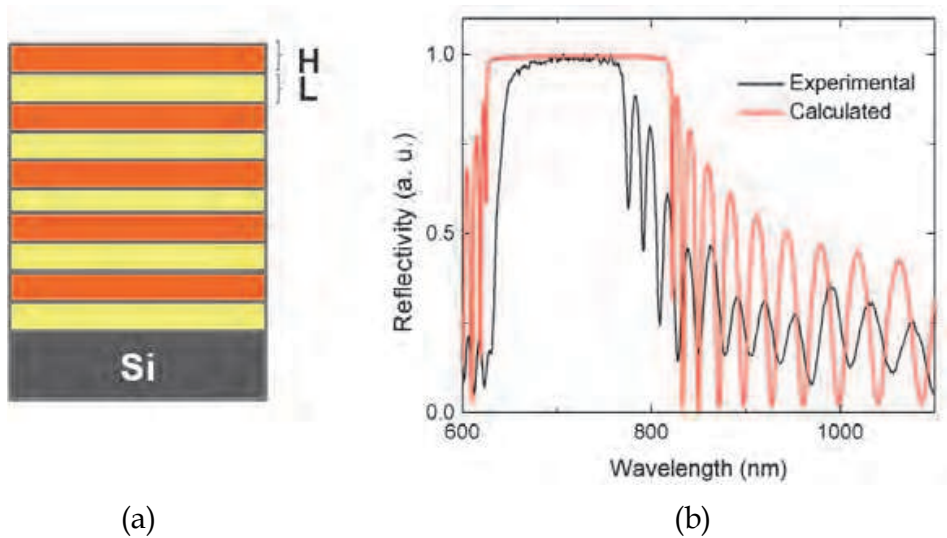

(a)   (b)

Fig. 9. (a) Schematic of a Bragg mirror. (b) Experimental normal incidence reflectivity spectrum from a Bragg mirror (black line) compared with the calculated one (red line).

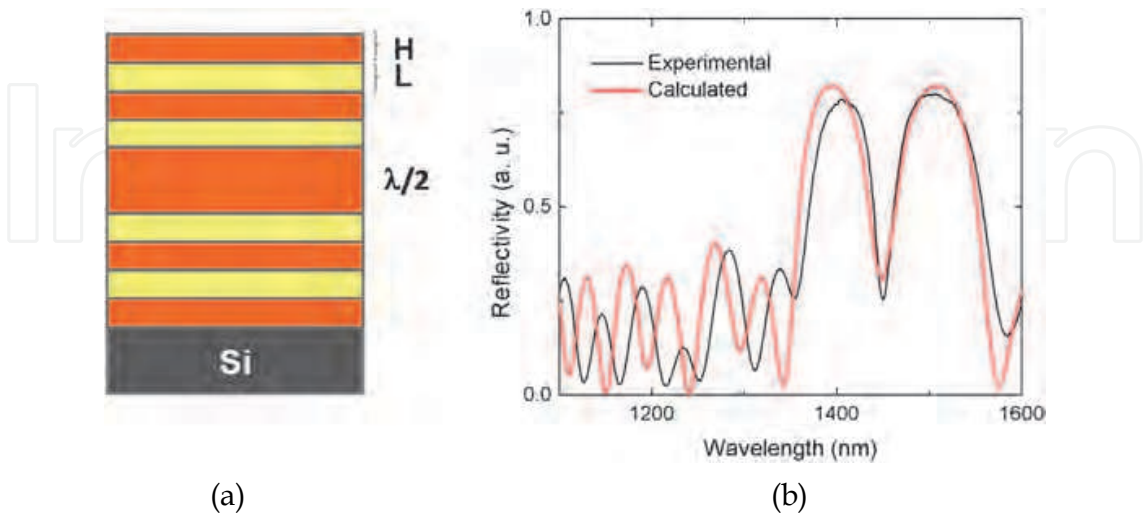(a)   (b)

Fig. 10. (a) Schematic of an optical microcavity. (b) Experimental normal incidence reflectivity spectrum of a microcavity (black line) compared with the calculated one (red line).

An optical microcavity is a $\lambda/2$ layer sandwiched between two distributed Bragg mirrors (Figure 10 (a)). The reflectivity spectrum of a microcavity is characterized by a transmittance peak in the photonic stop band (Figure 10 (b)). The Q factor of the microcavity is defined as $Q=\lambda/\Delta\lambda$, where λ is the wavelength of the resonance peak and $\Delta\lambda$ is the full width half maximum (FWHM) of the resonance. This parameter is used to evaluate how the light is confined in the PBG structure. The calculated reflectivity spectra of the structures reported in Figure 9 e 10 have been reproduced by a transfer matrix method (Muriel & Carballar, 1997), also taking into account the wavelength dispersion of the silicon refractive index.

3.3 Thue-Morse sequences

A quasi-crystal (QC) does not have a geometrical periodicity but is still deterministically generated. Even if these structures do not have a translational symmetry, they show several interesting physical properties such as the photonic band gaps, some resonance frequencies, and some high localized states (Soukoulis & Economou, 1982). Thue-Morse (T-M) (Liu, 1997) sequence is one of the most common examples of one dimensional QC. The T-M one dimensional structure is constituted by the sequence of two layers A and B with refractive index n_A (n_B) and thickness d_A (d_B). Applying the substitution rules A→AB and B→BA [26] all subsequent orders can be deduced, as follow: S_0=A, S_1=AB, S_2=ABBA, S_3=ABBABAAB, S_4=ABBABAABBAABABBA, and so on.
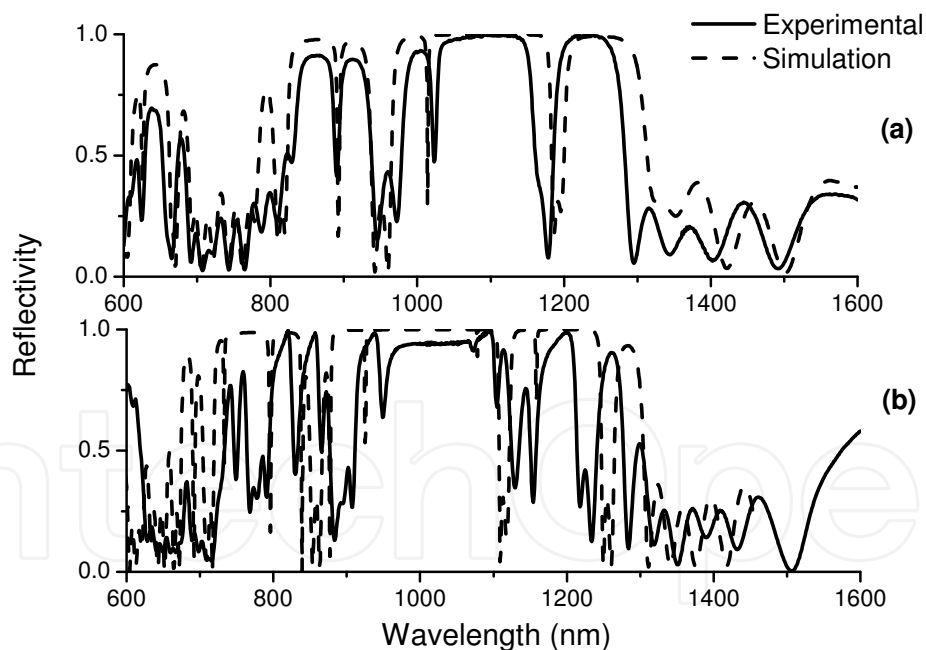

Fig. 11. Experimental (solid line) and calculate (dash line) reflectivity for S_6 T-M structure (a) and S_7 T-M structure (b). The measurements have been taken at normal incidence.

The layers number of S_N is 2N, where N is the T-M order. Dielectric T-M structures up to 128 layers have been fabricated by using PSi technology (Moretti et al., 2006). The high porosity layers are characterized by a porosity p_A=81%, with an average refractive index $n_A\cong1.3$ and a thickness $d_A\cong135$ nm.
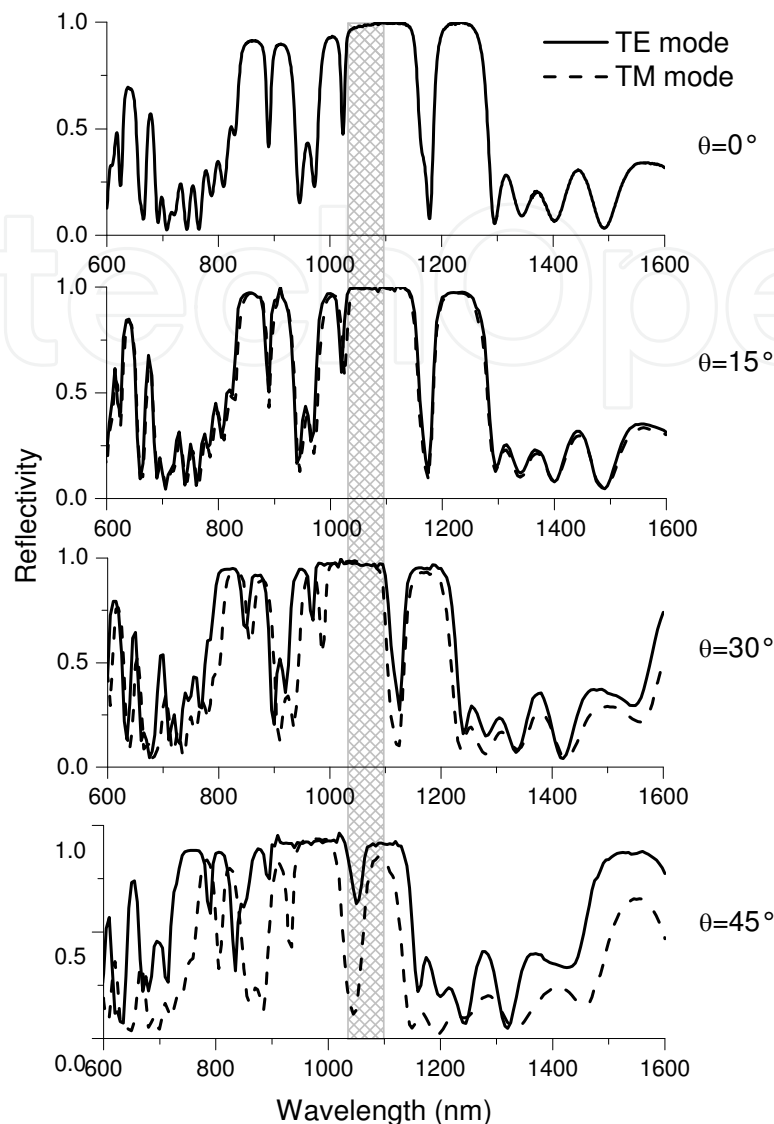
Fig. 12. Experimental reflectivity spectra of S_6 T-M structure for the transverse electric (TE) mode (solid line) and the transverse magnetic (TM) mode (dash line) for different incident angles.

The low porosity layers are characterized by a porosity p_B=56%, with a effective refractive index $n_B \cong 1.96$ and a thickness $d_B \cong 90$ nm. The thickness d_i of each layer was designed to satisfy the Bragg condition $n_i d_i = \lambda_0/4$ where n_i is the average refractive index and λ_0=700 nm. In Figure 11 the experimental (solid line) and calculated (dash line) reflectivity spectra are shown in case of S_6 (11-a), and S_7 (11-b) T-M structures. The good control in the fabrication process of the devices is demonstrated by the agreement between the measured and calculated spectra. The not perfect matching can be ascribed to non-uniformities of thickness and porosities of layers along the etching direction. The Figure 12 reports the experimental reflectivity spectra of the S_6 T-M structure for both the TE (solid line) and the TM (dash line) polarization for different incident angles up to 30°. The grey area highlights a PBG region of 70 nm, centred at 1100 nm which exists in the incident angle range between -30° and 30°.

4. Biochemical sensing based on porous silicon photonic devices

Biosensors are devices able to detect chemical and biological species or microorganisms. They can be used in many applications such as clinical diagnostics, environmental monitoring, and food quality control. A biosensor is constituted by a biomolecular probe, which can selectively recognize a biochemical target, immobilized on a transducer that converts the biological interaction into a signal. Different sensor platforms with remarkable detection properties, based on potentiometric, amperometric, magnetic and optical transducers have been developed. Among others, photonic sensing devices offer specific features which make them very attractive when not unique. Optical measurements are not invasive and can be used in harsh environments: they do not require electrical contacts that can cause explosions or fire. Opto-instrumentation is immune to electromagnetic interferences so that they are highly requested for applications where electrical currents could be harmful such as *in vivo* monitoring inside a patient body. Moreover, optical sensors are generally characterized by very short analysis time and high sensitivity. The optical detection principles are based either on fluorescence-labelled systems or on direct optical monitoring. Fluorescence detection has been the main approach in medical diagnostic, biotechnology and drug discovery for a long time. Recently, a new class of optical label-free sensors has been proposed, which uses direct optical methods (photoluminescence (Chan et al., 2001), surface plasmon resonance (SPR) (Homola et al., 1997; Jung et al., 1998), reflectivity (Mace et al., 2006), interference (Brandenburg & Henninger, 1994)) and label-free natural probes such as DNA sequences and proteins.
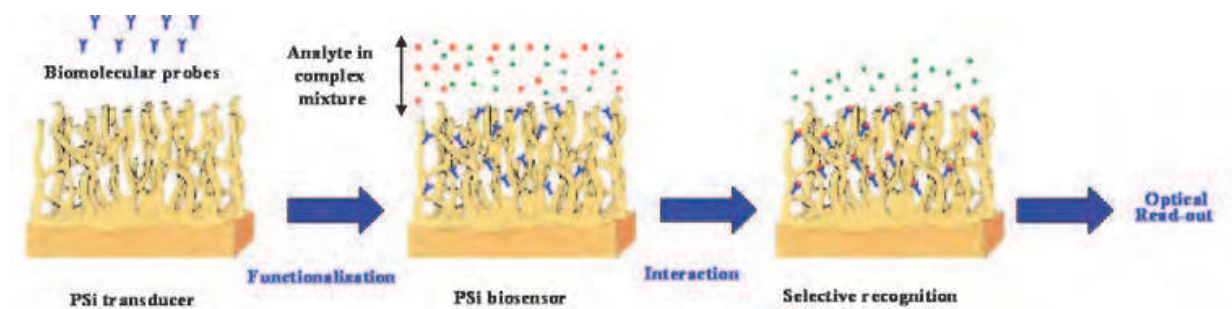

Fig. 13. A PSi biosensor is obtained immobilizing a biomolecular probe on the surface of a PSi transducer by using a proper functionalization process. The device is able to selectively recognize a target analyte in complex mixture.

The PSi is an ideal material as optical biosensor transducer since its large surface area can be easily modified by proper chemical passivation process. The label-free sensing mechanism is based on the change of the PSi refractive index on exposure to the substances to be detected, due to their infiltration into the pores; the consequence of the refractive index variation is a change in the reflectivity/transmittivity spectrum of the devices. The first measurement so far has been reported by Lin et al. who measured the shift of PSi Fabry-Perot fringes to detect the DNA hybridization (Lin et al., 1997). Since then, there has been a rapid growth of research activities in this area.

A key step in the fabrication of the PSi biosensor is the functionalization (*i.e.* covalent immobilization of the bioprobe) of its surface with the biological probe in order to make the device selective for the species of interest (Figure 13). The two main approaches used for the surface functionalization are the *ex situ* immobilization and the *in situ* synthesis.

4.1 *Ex situ* immobilization on PSi surface

The major drawback of the "as etched" PSi is its chemical instability: it is well known that the hydrogen-terminated PSi surface is slowly oxidized at room temperature by atmospheric oxygen, resulting in a blue shift of the optical spectrum (Canham, 1997). Moreover, it has been shown that a PSi device can be dissolved on exposure to alkaline solutions very often used in experiments of functionalization and biomolecular recognition (Anderson et al., 2003). The simplest method used to stabilize the PSi surface is the thermal oxidation of the structure. As already reported in section 2.4, the thermal oxidation at around 900°C completely oxidizes the PSi device inducing a reduction in pore diameter and porosity. Alternatively, a chemical oxidation in pyridine solution can be used: the process does not affect the pore size but it produces an oxide worse than the thermal one in terms of density and surface roughness. In both cases a change of the surface wettability, from hydrophobic to hydrophilic, is observed.
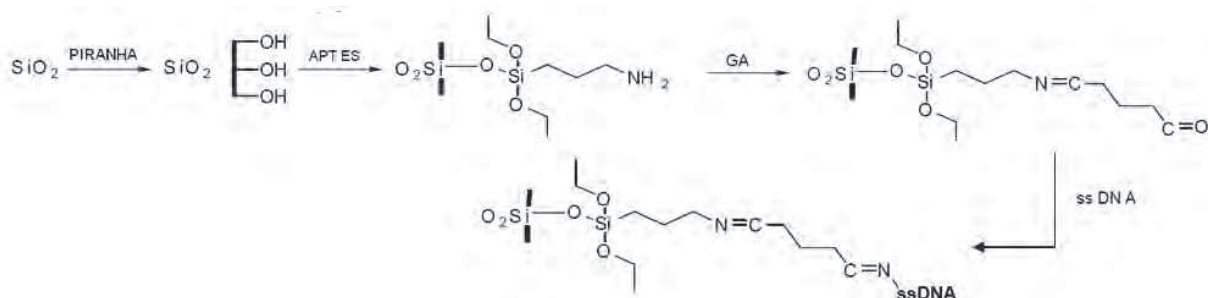

Fig. 14. Scheme of the functionalization process of a PSi Bragg mirror surface with DNA probe single strand (25 mer).

An example of surface functionalization with a bioprobe synthesized *ex situ* is reported in Figure 14. A PSi Bragg mirror, stabilized by means of a thermal oxidation at 900°C, was immersed in Piranha solution (4:1 sulfuric acid to hydrogen peroxide) for 40 min in order to assure the formation of Si-OH bonds. The chip was rinsed with deionized water and dried in a nitrogen stream. Then, the PSi surface was silanized in a 5 % solution of APTES (3-aminopropyltriethoxysilane) and anhydrous toluene for 30 min at room temperature. After the reaction time, the chip was washed twice in toluene to remove loosely physisorbed APTES, and baked at 100 °C for 10 min. The chip was thus immersed in a 2.5% glutaraldehyde (GA) solution in 20 mM HEPES buffer (pH 7.4) for 30 min. The GA reacts with the amino groups on the silanized surface and coats the internal surface of the pores with another thin layer of molecules. The PSi surface was incubated overnight at 4°C with a 200 µM amino terminated DNA single strand solution (30 µL).

From the optical point of view, the thermal oxidation causes blue-shifts of the reflectivity spectrum of the device of about 69 nm (Figure 15-b) due to the lower value of the SiO_2 refractive index (n_{ox}=1.46) with respect to the Si refractive index (n_{Si}=3.9). On the contrary, the functionalization steps (APTES+GA, and DNA probe) produce red shifts of the reflectivity spectra of 16 and 10 nm (Figures 15-c and 15-d), respectively, due to an increasing of the average refractive index of the layers.

4.2 *In situ* synthesis of oligonucleotides on PSi surface

The *in situ* synthesis of oligonucleotide (ON) on PSi surface is an alternative method to the traditional immobilization of DNA fragments. *In situ* technique allows to obtain high ON surface coverage and flexibility in the choice of the probe sequence.
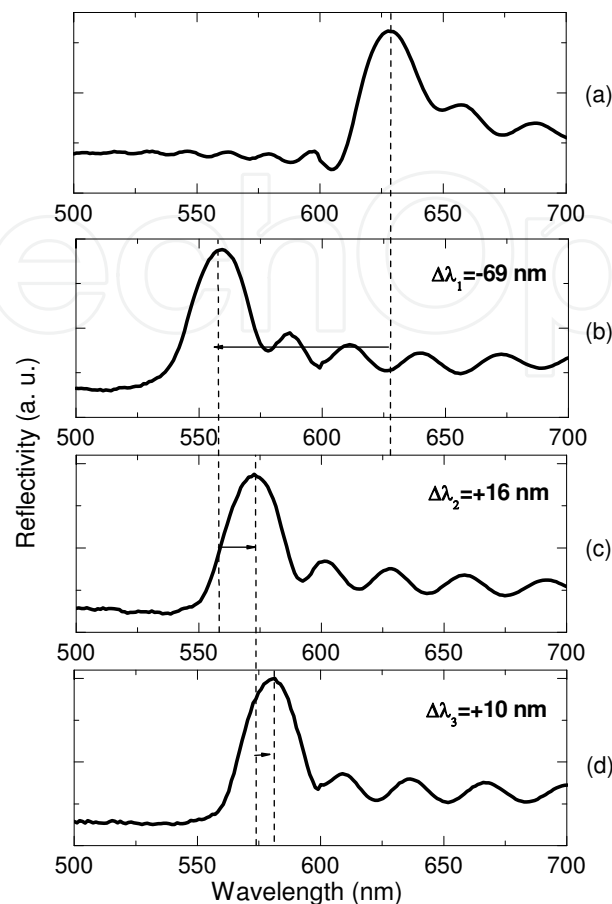
Fig. 15. Reflectivity spectra of the Bragg mirror before (a) and after (b) the thermal oxidation process, after the APTES and GA functionalization (c), and after the DNA probe immobilization (d).

Here, we report the ON synthesis on a PSi Bragg mirror obtained by alternating 20 high (H) refractive index layers (low porosity) and low (L) refractive index layers (high porosity) (Rea et al., 2010). The Bragg mirror was produced by electrochemical etching of highly doped p$^+$-silicon, <100> oriented, 0.003 Ω cm resistivity, 400 μm thick, using a HF (50% in weight):ethanol = 1:1 solution in the dark and at room temperature. A current density of 200 mA/cm^2 for 1.2 s was applied to obtain the low refractive index layers (n_L=1.542; d_L=125 nm) with a porosity of 72%, while a current density of 100 mA/cm^2 was applied for 1.4 s for the high index layers (n_H=1.784; d_H=108 nm) with a porosity of 64%. The structure has been thermally oxidized against uncontrolled environmental aging and corrosion in alkaline biological solutions. After the oxidation process, the PSi device was immersed in freshly prepared Piranha solution for 40 min at room temperature, rinsed with deionized water, and dried in a stream of nitrogen gas. This treatment creates Si-OH groups on the PSi surface. The structure was introduced in a suitable column reactor before the synthesis. DNA oligomer, constituted by thymine (T), was assembled on the chip following standard phosphoramidite chemistry by ten growing cycles thus obtaining polymer bound T10 (Figure 16).
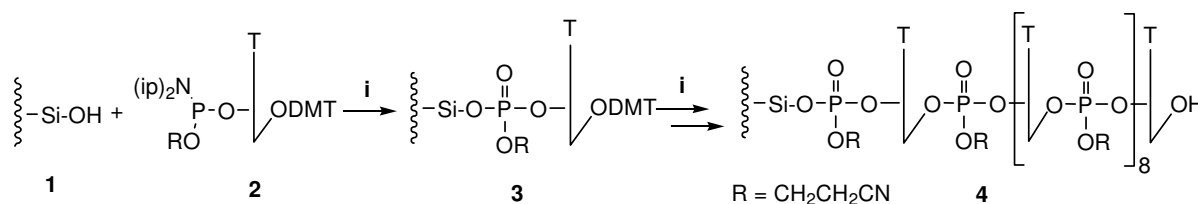
Fig. 16. Scheme of the solid phase synthesis of the 10 bases oligonucleotide **4** on the PSi-OH surface **1** using 5'-dimethoxytrityl-thymidine-phosphoramidite **2**; i: standard automatic synthetic cycle (Rea et al., 2010).

In order to quantify the surface functionalization, we have removed the 5'-dimethoxytrityl (DMT) protecting group from the support-bound 5'-terminal nucleotide by using the deblocking solution of trichloroacetic acid in dichloromethane (3% w/w). The release of the protecting group generates a bright red-orange colour solution in which the quantity of the DMT cation could be measured on-line by UV-VIS spectroscopy at 503 nm (ε = 71700 $M^{-1}cm^{-1}$). The Figure 17 shows the DMT analysis performed on the PSi device after each synthesis cycle: the amount of DMT indicated reaction yields over 98%. These values resulted almost steady during the ON growing process, confirming the stability of the chip surface and the high accessibility of ON 5'-OH end groups By averaging over these values, we have estimated a functionalization degree of 3.25 nmol/cm^2. The presence of ON chains bonded on the chip has been also verified by spectroscopic reflectometry. The biological molecules, attached to the PSi pore walls, induce an increase in the average refractive indexes of the layers, causing a red-shift in the reflectivity spectrum of the Bragg mirror. The magnitude of the shift increases with the increase of the pores surface coverage with the organic matter. The reflectivity spectra of the PSi multilayered structure before and after the ON synthesis are reported in Figure 18. A red-shift of 11 nm has been measured.
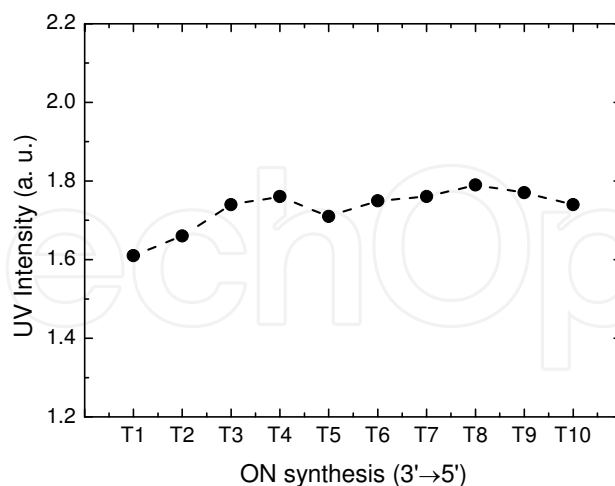

Fig. 17. DMT measurements performed on the sample after each synthesis cycle.

5. Integrated microfluidic porous silicon array

The microarray technology has demonstrated a great potential in drug discovery, genomics, proteomics research, and medical diagnostics (Pregibon et al., 2007; Poetz et al., 2005;
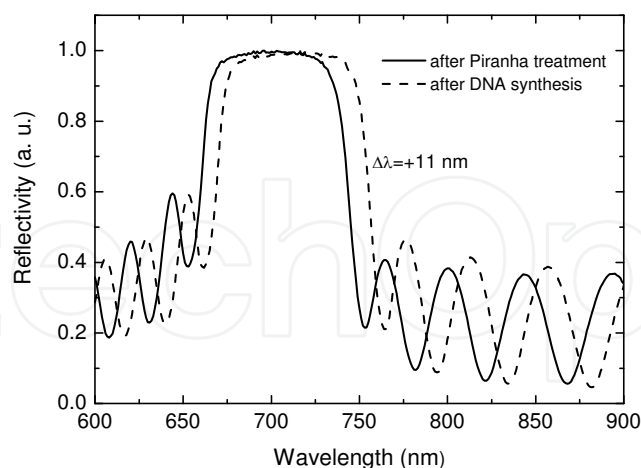
Fig. 18. Reflectivity spectra of the Bragg mirror before (solid line) and after (dash line) the oligonucleotide synthesis.

Nishizuka et al., 2003). The key issue is the very high throughput of these devices due to the large number of samples that can be simultaneously analyzed in a single parallel experiment. Further advantages are fast time analysis and the consumption of very small amount of reagents. The microarray technology is based on the immobilization of a large number of highly specific recognition elements on a solid platform. Different types of platform surfaces have already been explored; the most common examples are derivatized glass and gold/aluminium substrates (MacBeath & Schreiber, 2000; O'Connor & Pickard, 2003). Silicon, and silicon related materials, is by far the most important and diffuse material for lab-on-chip applications due to the high development of the integrated circuits technology. Recently, porous silicon substrates have been proposed for reverse phase protein and DNA microarray (Ressine et al., 2007; Chen et al., 2009; Yamaguchi et al., 2007): small sensing area with high detection efficiency is the key feature in both applications, in which quantitative signals are generated by fluorescence and infrared spectroscopy, respectively. Alternatively, we have studied the fabrication process and the optical characterization by reflectometry of a microarray of PSi photonic devices as functional platform for label-free detection of biomolecular interactions (Rea at al., 2010b). The array support has been integrated with a microfluidic circuit made of polydimethylsiloxane (PDMS) which strongly reduces the functionalization time, chemical and biological products consumption, while it preserves all the features of the PSi label-free optical detection.

5.1 Fabrication and optical characterization of the PSi Bragg mirror microarray

The integration of the PSi elements in a microarray is not straightforward. To this aim a proper technological process has been designed. The process flow chart of the PSi μ-array fabrication is schematized in Figure 1. The silicon substrate was a highly doped p+-type wafer with a resistivity of 0.01 Ω cm, <100> oriented and 400 μm tick. Silicon nitride has been used as masking material during the electrochemical etching since it shows a better resistance against the HF solution with respect to photoresist, which effectively protects the silicon only for 2-3 min (Tao & Esashi, 2004). The silicon nitride film, 1.6 μm thick, was deposited by PECVD on the substrate (Figure 19 (a)). A standard photolithographic process

was used to pattern the silicon nitride film (Figure 19 (b)), which has been subsequently etched by RIE process in CHF_3/O_2 atmosphere (Figure 19 (c)). Finally, the silicon wafer was electrochemically anodized in a HF-based solution (50 wt. % HF : ethanol = 1:1) in dark and at room temperature (Figure 19 (d)). We have realized the Bragg reflectors by alternating high (H) refractive index layers (low porosity) and low (L) refractive index layers (high porosity); a current density of 80 mA/cm² was applied to obtain low refractive index layers (n_L=1.6) with a porosity of 71 %, while one of 60 mA/cm² was applied for high index layers (n_H=1.69) with a porosity of 68 %. The device was then fully oxidized in pure O_2.
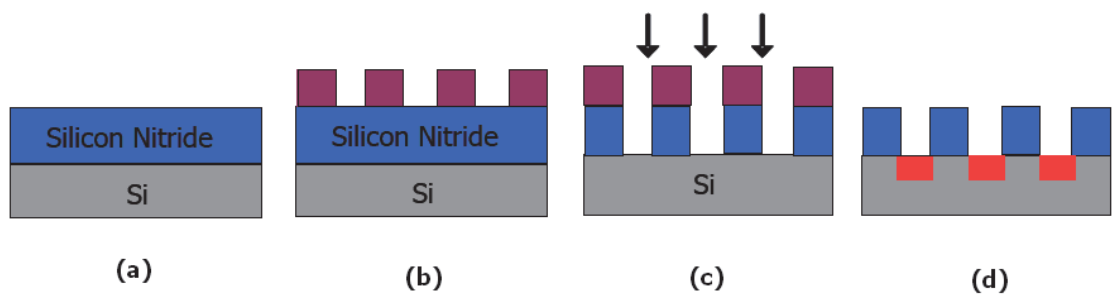

Fig. 19. Technological steps of the PSi μ-array fabrication process.

The optical microscope image of the microarray and the reflectivity spectra of some Bragg mirror elements are reported in Figure 20. The diameter of each element is of 200 μm, but it can be reduced to about 1 μm, by changing properly the photolithographic mask. The reflectivity spectra at normal incidence of the Bragg devices are characterized by a resonance peak at 627 nm and a FWHM of about 25 nm. The spectra demonstrate also the uniformity of the electrochemical etching on the whole microarray surface.
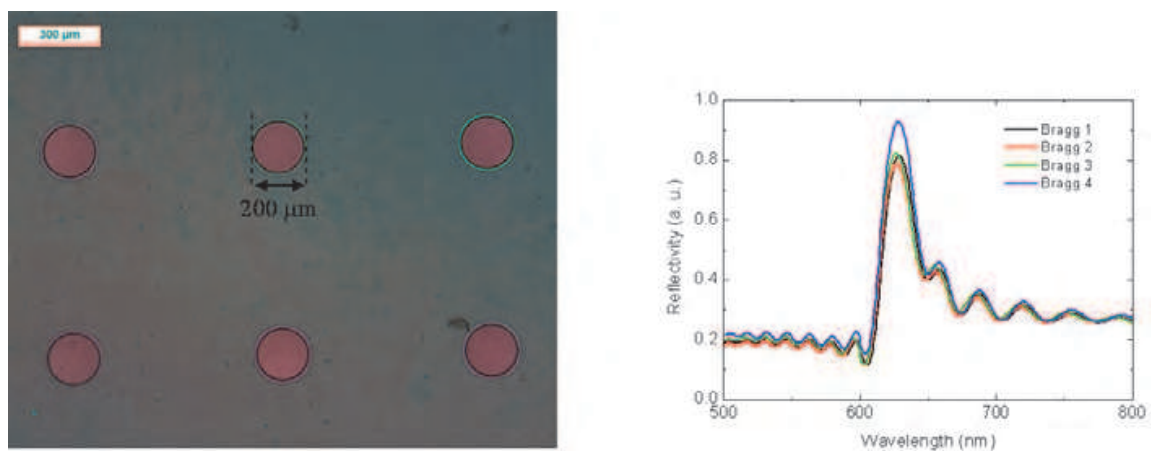

Fig. 20. Optical microscope image of the microarray and reflectivity spectra of the PSi Bragg mirrors.

5.2 Integration of the PSi array with a microfluidic system
The microfluidic system was designed by a computer aided design software. The pattern was printed 10 times bigger than its real size on a A4 paper by a laser printer (resolution 1200 dpi) and then transferred on a photographic film (Maco Genius Print Film) by a

photographic enlarger (Durst C35) reversely used. The designed fluidic system was replicated by photolithographic process on a 10-µm thick negative photoresist (SU-8 2007, MicroChem Corp.) spin-coated for 30 s at 1800 rpm on a silicon substrate. After the photoresist development (SU-8 developer, MicroChem Corp.), the silicon wafer was silanized on exposure to chlorotrimethylsilane (Sigma-Aldrich Co.) vapour for 10 min as anti-sticking treatment. A 10:1 mixture of PDMS prepolymer and curing agent (Sylgard 184, Dow Corning) was prepared and degassed under vacuum for 1 hour. The mixture was poured on the patterned wafer and cured on a hot plate at 75°C for 3h to facilitate the polymerization and the cross-linking process. After the PDMS layer peeling, inlet and outlet holes were drilled through it in order to allow the access of liquid substances to the system. Finally, the PDMS layer was rinsed in ethanol in a sonic bath for 10 min. The surfaces of PDMS layer and microarray, whose PSi elements were thermally oxidized, were activated by exposing to oxygen plasma for 10 sec to create silanol groups (Si-OH) as shown in the schematic reported in Figure 21, aligned under a microscope using an x-y-z theta stage, and sealed together. After the sealing with the PDMS system, the PSi elements of the array have been functionalized with DNA single strand, as described in section 4.1. The microfluidic circuit allows to use only few microlitres (~5 µl) of biologicals with respect to the tens of microlitres used in the case of not integrated devices. Moreover, the incubation time has been also reduced from eight to three hours. After the bio-functionalization with DNA probe, we have studied the DNA-DNA hybridization by injecting into the microchannel 200 µM of complementary sequence. Figure 22 shows the reflectivity spectra of a PSi Bragg mirror after the DNA functionalization and after the complementary DNA interaction. A red-shift of 5.0 nm can been detected after the specific DNA-DNA interaction. A negligible shift, less than 0.2 nm (data not reported in the figure), is the result of a control measurement which has been done exposing another functionalized microchannel to non-complementary DNA, demonstrating that the integrated PSi array is able to discriminate between complementary and non-complementary interactions.
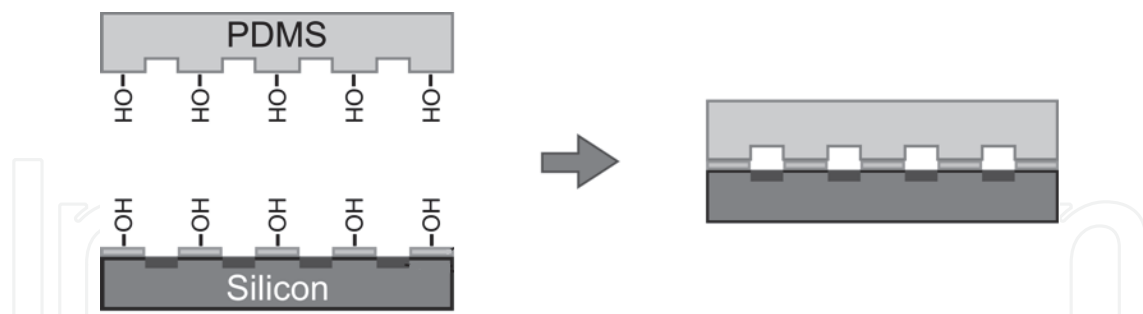

Fig. 21. Scheme of the fabrication process used to integrate the PSi array with a PDMS microfluidic system.

6. Conclusion

The PSi technology allows the fabrication of different multilayered devices with complex photonic features such as optical resonances and band gaps. These photonic structures, functionalized with a biomolecular probe able to selectively recognize a biochemical target, have been successfully used as label-free optical biosensors. The sensing mechanism is based on the increase of the PSi refractive index due to the infiltration of the biological
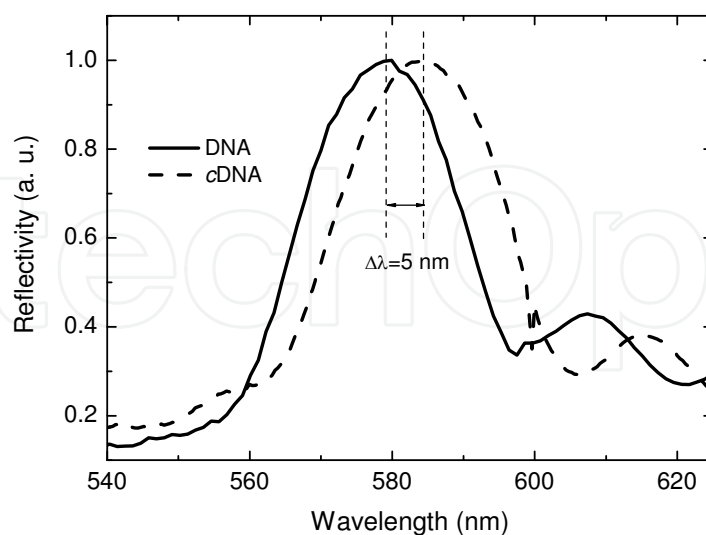
Fig. 22. Reflectivity spectra of a PSi Bragg mirror after the DNA probe attachment (solid line), and after the hybridization with the complementary DNA (dash line).

substances into the nanometric pores of the material; the consequence of the refractive index change is the shift of the reflectivity spectrum of the photonic devices. Since PSi technology is compatible with the microelectronic processes, it can be easily used as functional platform in the fabrication on integrated microsystems. As example, we have reported the realization of a PSi microarray for the detection of multiple DNA-DNA interactions. The array, characterized by a density of 170 elements/cm^2, has been integrated with a microfluidic system made of PDMS which allows to reduce the consumption of the chemical and biological substances.

7. References

Anderson, S.H.C.; Elliot, H.; Wallis, D.J.; Canham, L.T. & Powell, J.J. (2003). Dissolution of different forms of partially porous silicon wafers under simulated physiological conditions. *Phys. Status Solidi A*, Vol. 197, pp. 331-335.

Anderson, M.A.; Tinsley-Brown, A.; Allcock, P.; Perkins, E.A.; Snow, P.; Hollings, M.; Smith, R.G.; Reeves, C.; Squirrell, D.J.; Nicklin, S. & Cox, T.I. (2003). Sensitivity of the optical properties of porous silicon layers to the refractive index of liquid in the pores. *Phys. Stat. Sol. A*, Vol. 197, pp. 528-533.

Aspnes, D.E. & Theeten, J. B. (1979). Investigation of effective-medium models of microscopic surface-roughness by spectroscopic ellipsometry. *Physical Review B*, Vol. 20, pp. 3292-3302.

Brandenburg, A. & Henninger, R. (1994). Integrated optical Young interferometer. *Applied Optics*, Vol. 33, pp. 5941-5947.

Canham, L.T. (1990). Silicon quantum wire array fabrication by electrochemical and chemical dissolution of wafers. *Appl. Phys. Lett.,* Vol. 57, pp. 1046-1048.

Chan, S.; Horner, S.R.; Fauchet, P.M. & Miller, B.L. (2001). Identification of Crom Negative Bacteria using nanoscale silicon microcavities. *J. Am. Chem. Soc.*, Vol. 123, pp. 11797-11798.

Chandrasekaran, A.; Acharya, A.; You, J.L.; Soo, K. Y.; Packirisamy, M.; Stiharu, I. & Darveau, A. (2007). Hybrid integrated silicon microfluidic platform for fluorescence based biodetection. *Sensors*, Vol. 7, pp. 1901-1915.

Chen, L.; Chen , Z.T.; Wang , J.; Xiao , S.J.; Lu, Z.H.; Gu, Z.Z.; Kang, L.; Chen, J.; Wu, P.H.; Tang, Y.C. & Liu, J.N. (2009). Gel-pad microarrays templated by patterned porous silicon for dual-mode detection of proteins. *Lab on a Chip*, Vol. 9, pp. 756-760.

Dancil, K.P.S.; Greiner, D.P. & Sailor, M.J. (1999). A porous silicon optical biosensor: Detection of reversible binding of IgG to a protein A-modified surface. *J. Am. Chem. Soc.*, Vol. 121, pp. 7925-7930.

De Stefano, L.; Rendina, I.; Moretti, L. & Rossi, A.M. (2003). Optical sensing of flammable substances using porous silicon microcavities. *Mater. Sci. Eng. B*, Vol. 100, pp. 271-274.

Grosman, A. & Ortega, C. (1997). Chemical composition of 'fresh' porous silicon, In: *Properties of Porous Silicon*, Edited by L.T. Canham, pp. 145-153, INSPEC, London.

Homola, J.; Ctyroky, J.; Skalsky, M.; Hradilova, J. & Kolarova, P. (1997). A surface plasmon resonance based integrated optical sensor. *Sensors and Actuators B*, Vol. 39, pp. 286-290.

Jung, L.S.; Campbell, C.T.; Chinowsky, T.M.; Mar, M.N. & Yee, S.S. (1998). Quantitative interpretation of the response of surface plasmon resonance sensors to adsorbed films. *Langmuir*, Vol. 14, pp. 5636-5648.

Lehmann, V. & Gösele, U. (1991). Porous silicon formation: a quantum wire effect. *Appl. Phys. Lett.*, Vol. 58, pp. 856.

Lehmann, V. (2002). *Electrochemistry of Silicon*, Wiley-VCH Verlag GmbH & Co, pp. 17–20.

Lin, V.S.Y.; Motesharei, K.; Dancil, K.P.S.; Sailor, M.J. & Ghadiri, M.R. (1997). A porous silicon based optical interferometric biosensor. *Science*, Vol. 270, pp. 840.

Liu, N.H. (1997). Propagation of light waves in Thue-Morse dielectric multilayers. *Phys. Rev. B*, Vol. 55, pp. 3543-3547.

MacBeath, G. & Schreiber, S.L. (2000). Printing proteins as microarrays for high-throughput function determination. *Science*, Vol. 289, pp. 1760-1763.

Mace, C.R.; Striemer, C.C. & Miller, B.L. (2006). Theoretical and experimental analysis of arrayed imaging reflectometry as a sensitive proteomics technique. *Anal. Chem.*, Vol. 78, pp. 5578-5583.

Moretti, L.; Rea, I.; Rotiroti, L.; Rendina, I.; Abbate, G.; Marino, A. & De Stefano L. (2006). Photonic band gaps analysis of Thue-Morse multilayers made of porous silicon. *Optics Express*, Vol. 14, pp. 6264-6272.

Mulloni, V. & Pavesi, L. (2000). Porous silicon microcavities as optical chemical sensors. *Appl. Phys. Lett.*, Vol. 76, pp. 2523.

Muriel, M. A. & Carballar, A. (1997). Internal field distributions in fiber Bragg gratings. *IEEE Photonics Technol. Lett.*, Vol. 9, pp. 955-957.

Nishizuka, S.; Chen, S.T.; Gwadry, F.G.; Alexander, J.; Major, S.M.; Scherf, U.; Reinhold, W.C.; Waltham, M.; Charboneau, L.; Young, L.; Bussey, K.J.; Kim, S.Y.; Lababidi, S.; Lee, J.K.; Pittaluga, S.; Scudiero, D.A.; Sausville, E.A.; Munson, P.J.; Petricoin, E.F.; Liotta, L.A.; Hewitt, S.M.; Raffeld, M. & Weinstein, J.N. (2003). Diagnostic markers

that distinguish colon and ovarian adenocarcinomas: identification by genomic, proteomic, and tissue array profiling. *Cancer Research*, Vol. 63, pp. 5243-5250.

O'Connor, D.C. & Pickard, K. (2003). *Microarrays and Microplates: Applications in Biomedical Science*, Edited by S. Ye & I.N.M. Day, pp. 65-72, BIOS Scientific Publishers, Oxford.

Pap, E.; Kordás, K.; Tóth, G.; Levoska, J.; Uusimäki, A.; Vähäkangas, J.; Leppävuori, S. & George, T.F. (2005). Thermal oxidation of porous silicon: study on structure. *Appl. Phys. Lett.*, Vol. 86, pp. 041501.

Pickering, C.; Canham, L.T. & Brumhead, D. (1993). Spectroscopic ellipsometry characterization of light-emitting porous silicon structures. *Appl. Sur. Sci.*, Vol. 63, pp. 22-26.

Pirasteh, P.; Charrier, J.; Soltani, A.; Haesaert, S.; Haji, L.; Godon, C. & Errien, N. (2006). The effect of oxidation on physical properties of porous silicon layers for optical applications. *Applied Surface Science*, Vol. 253, pp. 1999-2002.

Poetz, O.; Ostendorp, R.; Brocks, B.; Schwenk, J.M.; Stoll, D.; Joos, T.O.; Templin, M.F. (2005). Protein microarrays for antibody profiling: Specificity and affinity determination on a chip. Proteomics, Vol. 5, pp. 2402-2411.

Pregibon, D.C. ; Toner, M. & Doyle, P.S. (2007). Multifunctional encoded particles for high-throughput biomolecule analysis. *Science*, Vol. 315, pp. 1393-1396.

Rea, I.; Oliviero, G.; Amato, J.; Borbone, N.; Piccialli, G.; Rendina, I. & De Stefano L. (2010). Direct synthesis of oligonucleotides on nanostructured silica multilayers. *The Journal of Physical Chemistry C*, Vol. 114, pp. 2617-2621.

Rea, I.; Lamberti, A.; Rendina, I.; Coppola, G.; De Tommasi, E.; Gioffrè, M.; Iodice, M.; Casalino, M. & De Stefano L. (2010b). Fabrication and characterization of a porous silicon based microarray for label-free optical monitoring of biomolecular interactions. *Journal of Applied Physics*, Vol. 107, pp. 014513.

Ressine, A.; Corin, I.; Järås, K.; Guanti, G.; Simone, C.; Marko-Varga, G. & Laurell, T. (2007). Porous silicon surfaces - A candidate substrate for reverse protein arrays in cancer biomarker detection. *Electrophoresis*, Vol. 28, pp. 4407-4415.

Ruike, M.; Houzouji, M.; Motohashi, A.; Murase, N.; Kinoshita, A. & Kaneko, K. (1996). Pore structure of porous silicon formed on a lightly doped crystal silicon. *Langmuir*, Vol. 12, pp. 4828-4831.

Sing, K.S.W.; Everett, D.H.; Haul, R.A.W.; Moscou, L.; Pierotti, R.A.; Rouquerol, J. & Siemieniewska, T. (1985). Reporting physisorption data for gas solid systems with special reference to the determination of surface-area and porosity. *Pure Appl. Chem.*, Vol. 57, pp. 603-619.

Smith, R. L. & Collins, S. D. (1992). Porous silicon formation mechanisms. *J. Appl. Phys.*, Vol. 71, R1.

Snow, P.A.; Squire, E.K.; Russell, P.S.J. & Canham, L.T. (1999). Vapor sensing using the optical properties of porous silicon Bragg mirrors. *J. Appl. Phys.*, Vol. 86, pp. 1781.

Soukoulis, C.M. & Economou, E.N. (1982). Localization in one-dimensional lattices in the presence of incommensurate potentials. *Phys. Rev. Lett.*, Vol. 48, pp. 1043-1046.

Tao, Y. & Esashi, M. (2004). Local formation of macroporous silicon through a mask. *J. Micromech. Microeng.*, Vol. 14, pp.1411-1415.

Tompkins, H. G. & McGaham, W. A (1999). *Spectroscopic Ellipsometry and Reflectometry*. Ed. John Wiley & Sons.

Uhlir, A. (1956). Electrolytic Shaping of Germanium and Silicon. *The Bell System Technical Journal*, Vol. 35, pp. 333-347.

Xia, Y. & Whitesides, G.M. (1998). Soft lithography. *Annu. Rev. Mater. Sci.*, Vol. 28, pp.153-184.

Yamaguchi, R.; Miyamoto, K.; Ishibashi, K.; Hirano, A.; Said, S.M.; Kimura, Y. & Niwano, M. (2007). DNA hybridization detection by porous silicon-based DNA microarray in conjugation with infrared microspectroscopy. *J. Appl. Phys.*, Vol. 102, Article num. 014303.

Yon, J.J.; Barla, K.; Herino, R. & Bomchil, G. (1987). The kinetics and mechanism of oxide layer formation from porous silicon formed on p-Si substrates. *J. Appl. Phys.*, Vol. 62, pp. 1042-1048.

Zangooie, S.; Jansson, R. & Arwin, H. (1999). Ellipsometric characterization of anisotropic porous silicon Fabry-Perot filters and investigation of temperature effects on capillary condensation efficiency. *J. Appl. Phys.*, Vol. 86, pp. 850-858.

Zangooie, S.; Bjorklung, R. & Arwin, H. (1998). Protein adsorption in thermally oxidized porous silicon layers. *Thin Solid Films*, Vol. 313, pp. 825-830.
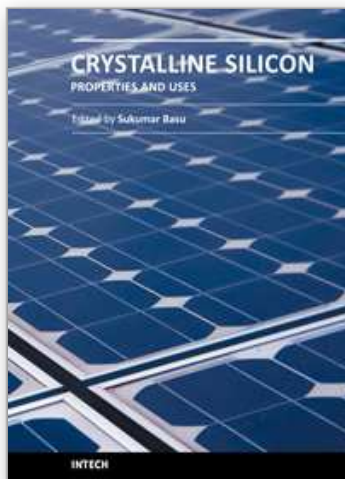
Crystalline Silicon - Properties and Uses

Edited by Prof. Sukumar Basu

The exciting world of crystalline silicon is the source of the spectacular advancement of discrete electronic devices and solar cells. The exploitation of ever changing properties of crystalline silicon with dimensional transformation may indicate more innovative silicon based technologies in near future. For example, the discovery of nanocrystalline silicon has largely overcome the obstacles of using silicon as optoelectronic material. The further research and development is necessary to find out the treasures hidden within this material. The book presents different forms of silicon material, their preparation and properties. The modern techniques to study the surface and interface defect states, dislocations, and so on, in different crystalline forms have been highlighted in this book. This book presents basic and applied aspects of different crystalline forms of silicon in wide range of information from materials to devices.

How to reference

In order to correctly reference this scholarly work, feel free to copy and paste the following:

Emanuele Orabona, Ivo Rendina, Luca De Stefano and Ilaria Rea (2011). Porous Silicon Integrated Photonic Devices for Biochemical Optical Sensing, Crystalline Silicon - Properties and Uses, Prof. Sukumar Basu (Ed.), ISBN: 978-953-307-587-7, InTech, Available from: http://www.intechopen.com/books/crystalline-silicon-properties-and-uses/porous-silicon-integrated-photonic-devices-for-biochemical-optical-sensing

INTECH
open science | open minds